Bio-Medical Materials and Engineering 29 (2018) 95–108
DOI 10.3233/BME-171715
IOS Press

Numerical simulation of low-density lipoprotein mass transport in human arterial stenosis – Calculation of the filtration velocity

Fatemeh Karami *, Siamak Hossainpour and Farzan Ghalichi
Department of Mechanical Engineering, Sahand University of Technology, Sahand New Town, East Azarbayjan, Tabriz, Iran
E-mails: karamif.mech@gmail.com, hossainpour@sut.ac.ir, fghalichi@sut.ac.ir

Received 8 February 2017
Accepted 18 October 2017

Abstract. Accumulation of cholesterol and other atherogenic lipids such as low-density lipoprotein (LDL) in artery wall causes reduction of vessel diameter and artery stenosis. The study of the mass transfer of these large molecules in the wall with considering effective factors on lumen flow and different physiological factors is the subject considered nowadays. In this paper, results of two dimensional and axi-symmetric simulations of three different models of the artery with 60% stenosis under pulsatile blood flow are presented. Filtration velocity of LDL mass transport in the permeable artery wall and shear stress of blood flow are investigated using ADINA software Three different flow models are considered. In the first and second models, the filtration velocity considered as a given parameter and constant in arterial wall boundary, while in third model arterial wall considered as porous wall, the filtration velocity is calculated from pressure difference as an input parameter of the model. The results show that filtration velocity is strongly depend on geometry and it is not constant along the wall, contrary to simplified models. The results of concentration variations in lumen and wall illustrate the increase in near wall LDL concentration or concentration polarization.

Keywords: Low-density lipoprotein transport, arterial wall, fluid-structure interaction, filtration velocity, porous media

Abbreviations

C	LDL concentration
D	LDL diffusivity
$\vec{d}$	displacement vector
$\dot{\vec{d}}_s$	velocity vector within solid region
h^d	virtual quantity of the solid displacement
J	fluid element Jacobian
p	hydraulic pressure

* Corresponding author. Tel.: +983157722898; E-mail: karamif.mech@gmail.com.

∇p	pressure drop across arterial wall
R_0	radius of lumen domain
t	time
u	axial velocity
v	vertical velocity
$\vec{v}_f$	fluid velocity vector
β	Forchheimer coefficient
γ	effective deformation rate
κ	fluid permeability
λ	cross sectional area reduction of stenosis
μ	viscosity
μ_∞	lower value of the viscosity in Carreau model
μ_0	upper value of the viscosity in Carreau model
ρ	density
$\vec{\tau}$	stress vector
τ_s^{total}	total Cauchy stress
φ	porosity

Subscripts

f	refers to fluid region
p	refers to porous media
s	refers to solid region
w	refers to arterial wall
$_0$	refers to the quantities at the initial reference configuration

1. Background

Accumulation of cholesterol and other atherogenic lipids such as LDLs in artery wall causes to vessel diameter reduction and artery stenosis that play a major role in Atherosclerosis [1,2]. The study of the mass transfer of these large molecules in the wall has stimulated lots of interest. Most of these studies are classified into three categories: wall-free, fluid-wall, and multilayer models [3]. Wall-free model is the simplest one that the arterial wall is simplified by suitable boundary conditions. This model needs many parameters such as the mass transfer coefficient of the wall and filtration velocity. The fluid-wall model provides more information about concentration profiles on the wall because it includes both fluid and wall. The most complex models are multilayer models where the wall includes several layers with particular properties. The multilayer models provide the most realistic information about LDL transport in the arterial wall.

Fatouraee *et al.* [4] have investigated LDL transport in a wall-free model under both steady state and pulsatile flow conditions. Nematollahi *et al.* [5] have applied the same model to investigate the effects of non-Newtonian blood fluid for steady state flow. Prosi *et al.* [3] have used several mathematical models and focused on the study of the accumulation of LDL in arterial wall considering a highly disturbed flow. Their results confirm that the geometrical parameters such as curvature of the lumen section strongly

influence the accumulation of LDL in the arterial wall. Ai and Vafai [6] have proposed a new multilayer model based on porous media theory and experimental data for studying LDL transport in the blood stream and arterial wall. Yang and Vafai [7] have proposed a four-layer model to study the effects of hypertension. They have used five different categories of boundary conditions and pulsation on LDL transport in the lumen and the wall.

2. Objective

In this paper, three different models of artery have been utilized. These models are axisymmetry with 60% stenosis. The first example (wall-free) is simulated in ADINA CFD where the wall is simplified by boundary conditions. The two last models considering fluid and structure interaction are simulated in ADINA CFD and ADINA STRUCTURE softwares. We focus on the study of LDL transport in the arterial wall and investigate effects of shear stress and blood flow on LDL transport in the wall. Furthermore, in most of the presented models, the filtration velocity is considered as known parameter. In the last model, the filtration velocity is caculated using observed pressure difference as input.

3. Methods

All these models consider vessel blood flow as an axisymmetric tube with a 60% arterial stenosis. The basic model is shown in Fig. 1 [8]. In this figure, L_i is the upstream length proximal to the constriction and L_o is the distal length downstream from the stenosis. The shape of the stenosis is described by Eq. (1).

$$R(x) = 1 - \lambda e^{-\zeta x^2} \tag{1}$$

Where $\xi = 5$, $0.163 \leqslant \lambda \leqslant 0.368$ and $|x| \leqslant 4$. λ is the cross-sectional area reduction of stenosis $[(A_i - A_s)/A_i]$ and in the present study is set to 0.368 [9].

The blood is considered as a homogenous incompressible fluid. The blood flow in the arterial lumen is described by the continuity, momentum, and mass transfer equations

$$\nabla \cdot \vec{u} = 0 \tag{2}$$

$$\rho \frac{D\vec{u}}{Dt} = -\nabla p + \mu \nabla^2 \vec{u} \tag{3}$$

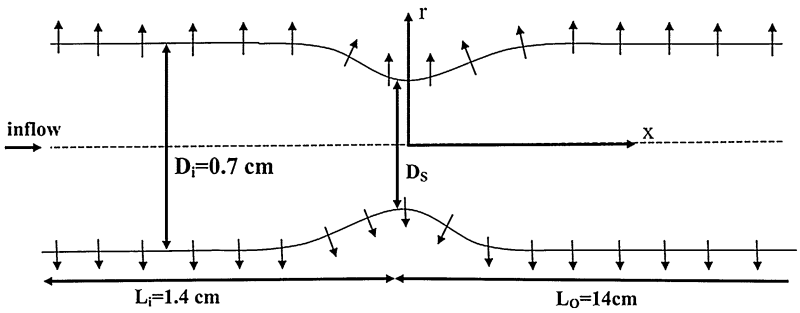

Fig. 1. Geometry of the axisymmetric arterial stenosis.

$$\frac{\partial C}{\partial t} + \vec{u} \cdot \nabla C = D\nabla^2 C \tag{4}$$

where $\vec{u}$ is the velocity vector, p is the hydraulic pressure, C is the LDL concentration, ρ, μ, and D are the fluid density, the dynamic viscosity, and the diffusivity coefficients, respectively.

The Carreau model for the non-Newtonian fluid is used [10].

$$\mu = \mu_\infty + (\mu_0 - \mu_\infty)\left(1 + (\mathrm{A}\gamma)^2\right)^n \tag{5}$$

Where μ_∞ and μ_0 are the lower and upper values of the viscosity in Carreau model taken as 0.0345 gr/cm s and 0.56 gr/cm s, respectively. A and n are the constant values set to 3.313 s and -0.5316, respectively, and γ is the effective deformation rate [11].

In the first model, the wall is simplified with suitable conditions described following.

A fully developed velocity profile is used at the inlet

$$u^*(0, r, t) = 2u(t)\left(1 - \left(\frac{r}{R_0}\right)^2\right), \quad 0 \leqslant r \leqslant R_0 \tag{6}$$

where $u(t)$ is the time-dependent mean velocity approximated by first 17 harmonic wave functions of carotid artery shown in Fig. 2 [4], and R_0 is the lumen radius.

The other initial and boundary conditions are given in Eq. (7).

$$\begin{aligned} &u(x, R_0, t) = 0, \qquad v(x, R_0, t) = v_w, \\ &u(0, r, t) = u^*, \qquad C(0, r, t) = C(x, r, 0) = 1 \end{aligned} \tag{7}$$

The first two conditions are no-slip and permeable wall conditions, respectively. The last three conditions are the inlet velocity, concentration boundary conditions, and concentration initial condition. At the inlet, the flow is assumed unidirectional, and the amount of the concentration is assumed uniform.

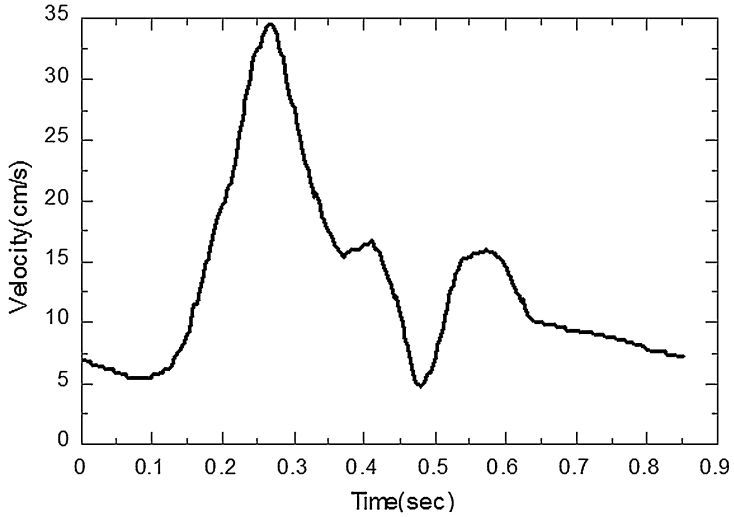

Fig. 2. Time dependent velocity at inlet [4].

Since no LDL can pass through the arterial wall, the balance between convective and diffusive transport at the luminal surface is determined as follows:

$$D\frac{\partial C}{\partial n} = C_w v_w \tag{8}$$

where v_w is the filtration velocity and set to 4×10^{-6} cm/s [12].

The second model is a fluid-wall model and includes a fluid and solid domain that considers fluid-structure interaction and 60% stenosis described by Eq. (1).

The governing equations of the fluid including conservation of mass, momentum and mass transfer equations are demonstrated by Eqs (1)–(5).

All of the fluid boundary conditions are the same as the conditions applied for previous model (Eqs (7) and (8)) but structure's one degree of freedom requires additional boundary condition as a time-dependent pressure in inlet shown in Fig. 3 [13,14].

The wall is modeled as the elastic solid with Yang's modulus, 6 MPa, Poisson's ratio of 0.45, and constant density of 1.057 gr/cm^3 [7,15]. The solid movement allowed just in the radial direction while one point from the wall is fixed in space (see Fig. 4). The kinematic, dynamic, and no-slip conditions are also applied to the fluid-structure interfaces [16].

$$\vec{d}_s = \vec{d}_f \tag{9}$$

$$n \cdot \vec{\tau}_f = n \cdot \vec{\tau}_s \tag{10}$$

$$\vec{v}_f = \dot{\vec{d}}_s \tag{11}$$

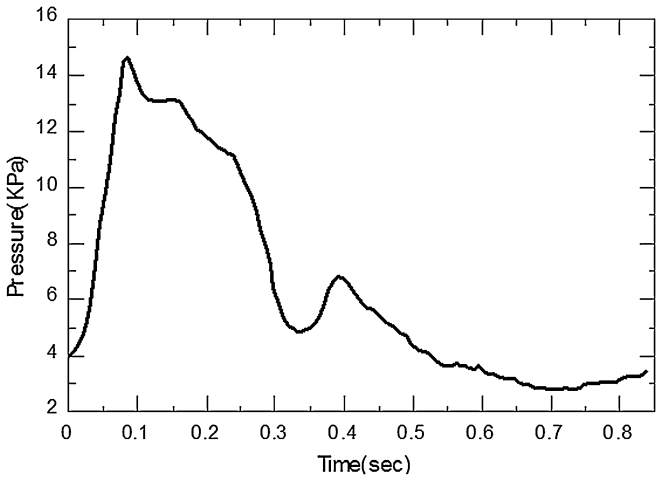

Fig. 3. Time dependent pressure at inlet [15].

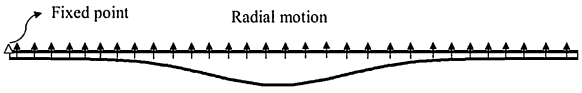

Fig. 4. The applied boundary conditions for solid model.

where $\vec{d}_f$ and $\vec{d}_s$ are the fluid and solid displacements, $\vec{\tau}_f$ and $\vec{\tau}_s$ are the fluid and solid stresses, respectively, and $\vec{v}_f$ is the fluid velocity. In ADINA8.8 software, the fluid and solid models are coupled and by the kinematic conditions, the nodal positions of the fluid on the common interfaces of the fluid and the structure are determined according to the dynamic condition, the fluid force along the interfaces is obtained by integrating of the fluid traction and exerting it on the structural node [16].

$$\overrightarrow{F(t)} = \int h^d \vec{\tau}_f \cdot \overrightarrow{ds} \tag{12}$$

where h^d is the virtual quantity of the solid displacement.

The third model is a fluid-wall model and includes three domains: lumen fluid, porous solid, and fluid through a porous medium. In this model, besides coupling of the lumen fluid and the solid on their common interface, the porous solid and fluid through a porous medium are coupled.

The governing equations of fluid are the same equations of the fluid as two former models. The fluid through porous medium is described by continuity and Darcy-Forchheimer equations [17–19]

$$\nabla \cdot u_p = 0 \tag{13}$$

$$\nabla p = -\beta\rho|u_p|u_p - \frac{\mu_p}{\kappa}u_p \tag{14}$$

Where u_p and μ_p are velocity and dynamic viscosity of fluid in a porous medium, respectively. κ and β are permeability of fluid and Forchheimer coefficient, respectively.

Unlike the former model that fluid-structure interaction are only applied on the common interface of solid and fluid, in this example, the fluid and structural variables are coupled to the entire porous medium.

The total Cauchy stress [20] in the solid model is given by Eq. (15).

$$\tau_s^{\text{total}} = \tau_s - pI \tag{15}$$

Where $-pI$ is the microscopic fluid stress added to the structural model. Equation (9) governs the whole porous medium as fluid, and solid displacements are equal. Considering the deformation of the wall, the porosity and accordingly its permeability could be changed. In ADINA software with assuming that the volume change of solid model is much smaller than the fluid model, the porosity and permeability of fluid are obtained by the following equations:

$$\phi = 1 - \frac{J_0}{J}(1 - \phi_0) \tag{16}$$

$$\kappa = \frac{\phi}{\phi_0}\kappa_0 \tag{17}$$

Where ϕ, J, and κ are the porosity, geometrical element Jacobian, and fluid permeability, respectively. Subscript 0 in all mentioned parameters indicate to the quantities at the initial reference configuration. The values of the main parameters required for solid and fluid are provided in Table 1. Media layer of

Table 1
The values of key parameters required of solid and fluid for the third model

	The first model	The second model	The third model
Number of the grids for fluid model	45115 square elements	18000 square element	20668 triangular elements
Number of the grids for solid model		360 square element	1280 square elements
Number of the cycles	140	5	one cycle
Convergence criterion	10^{-6}	10^{-6}	10^{-6}
Maximum number of iterations	1000	1000	1000
Maximum number of fluid-structure iterations		50000	50000
Time step (s)	0.05	0.002	0.002

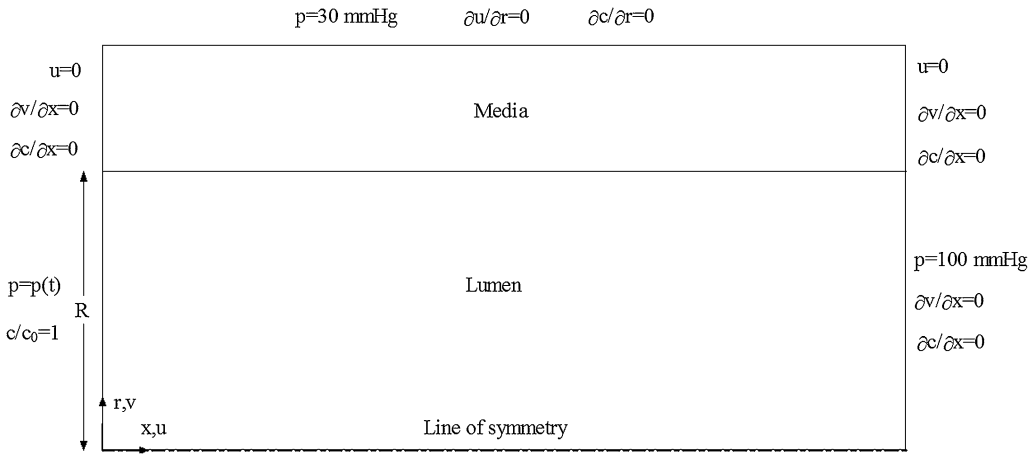

Fig. 5. The computation domain of the third model.

the blood vessel is the thickest layer, therefore, its property is implemented for the other layers. The chemical reactions are neglected in this layer.

Figures 4 and 5 show the boundary conditions of solid and fluid, respectively. Inlet time-dependent pressure is shown in Fig. 3. Unlike two previous models for the porous wall, filtration velocity is an unknown variable and must be calculated. Similar to the former model, the boundary conditions of FSI described by Eqs (9)–(11) are applied on the common interface of solid and fluid into the lumen.

The calculation is carried out using ADINA8.8 software based on finite element method which are applied for all models. The differential equations are solved by the Newtonian-Raphson iterative method.

For the first model, the size of grids near the wall is reduced where there is a high gradient of variables. This size changing is not applied to the second and third models with FSI condition, because some mesh elements become very deformed in FSI analysis. To investigate this problem, we reduced the size of grids in whole stenosis region. The concentration field gets steady periodic state after 140 cycles for the first model. The solution process for two other models takes more time and for this reason, the results are obtained for fewer cycles.

The parameters required for mesh configuration and numerical solution such as grid numbers, convergence criterion, time step, and periodic time are shown in Table 2.

Table 2
The parameters required for mesh configuration and numerical solution for the third model [8,9]

	Lumen	Media
Density, ρ (kg/cm^3)	1.05	1.057
Diffusivity, D (cm^2/s)	2.867×10^{-7}	5×10^{-10}
Elasticity (MPa)		6
Permeability, κ_0 (cm^2)		2×10^{-14}
Porosity, ϕ_0		0.258
Thickness (cm)	0.35	0.0214
Viscosity, μ (kg/cm s)	0.035	0.0072

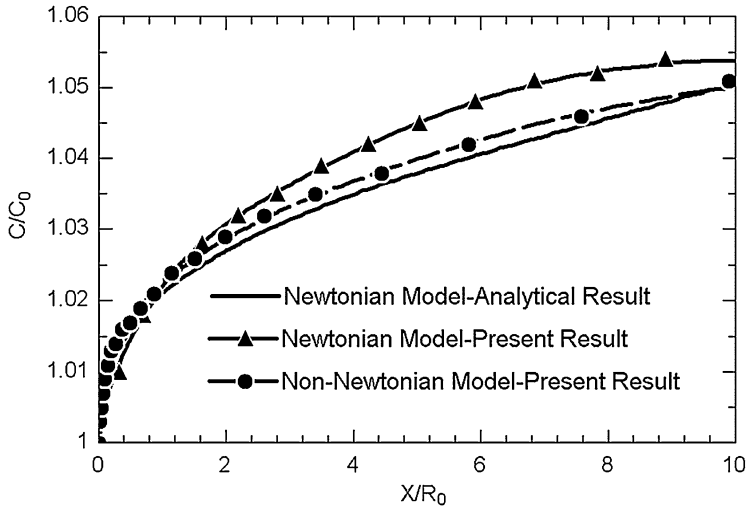

Fig. 6. The comparison of LSC variations along a simple geometry of arterial wall with analytical solution of Johnson *et al.* [13].

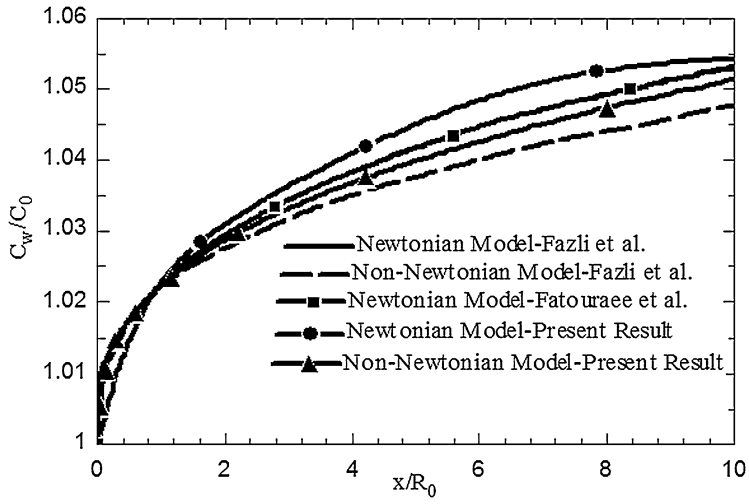

Fig. 7. Comparison of LSC variations for a simple tube.

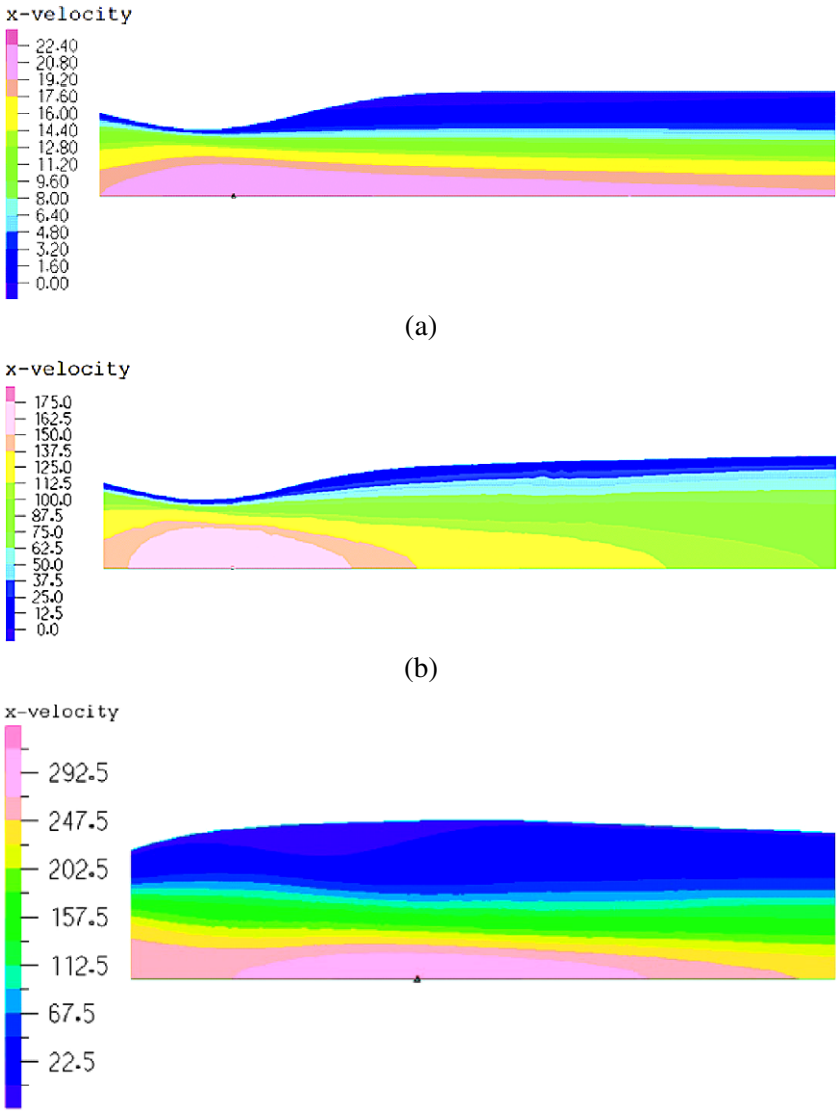

Fig. 8. Velocity contour at peak velocity in inlet (a) first model (b) second model (c) third model.

4. Results

To validate the applied numerical method, the Newtonian and non-Newtonian fluids in a simple artery under steady state flow are compared with the analytical solution of Johnson *et al.* [21] for a Newtonian fluid. The analytical results confirm the simulation results illustrated in Fig. 6. In Fig. 7 lumen surface concentration (LSC) under pulsatile flow are also compared with the numerical solution of Fatouraee *et al.* [4] and Fazli *et al.* [22]. As Figs 6 and 7 show, due to the concentration polarization phenomenon, a thin concentration boundary is formed in the length of arterial wall [23]. Figure 8 illustrates the velocity profile of the Newtonian fluid for all of the models in maximum inlet velocity time. The results show that the Reynolds number reaches a critical number and consequently a vortex is formed distal to stenosis in

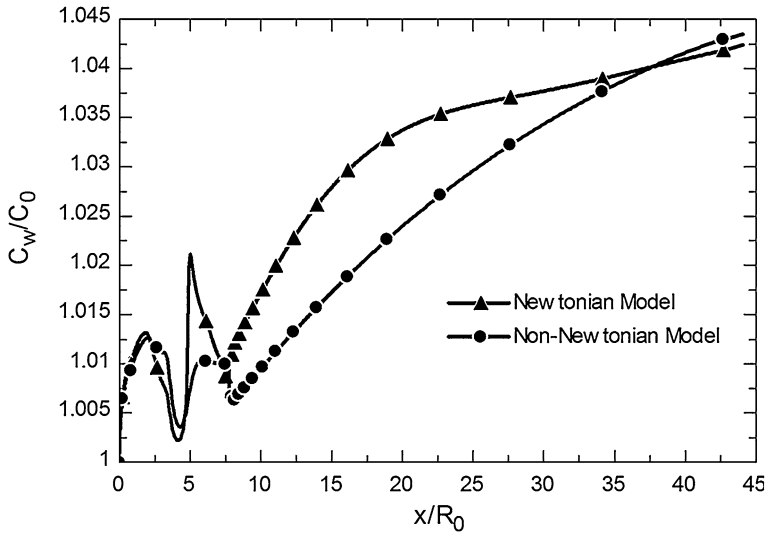

Fig. 9. Axial LSC variations for the wall-free Newtonian and non-Newtonian models.

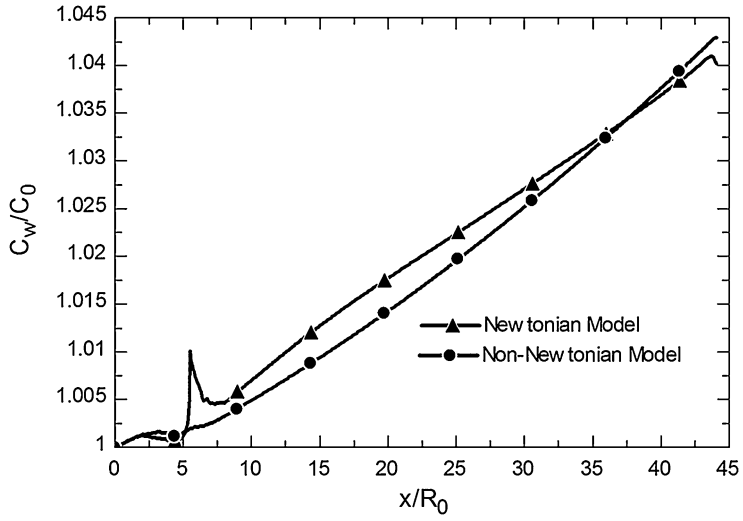

Fig. 10. Axial LSC variations for the fluid-wall Newtonian and non-Newtonian models.

the wall-free model (Fig. 8(a)). According to the velocity profile shown in Figs 8(b) and 8(c), no vortex is formed distal to stenosis for fluid-wall models, although the amount of shear stress decreases in this region. It seems that the wall motion prevents the vortex formation.

The mean LSC variations in the wall for all three models are shown in Figs 9–11, respectively. As can be seen, a thin layer is formed close to wall for all three models.

However, in the wall-free model, the concentration arbitrates high amount distal to stenosis where the flow separation point occurs, and the shear stress vanishes. Same variations are seen for the second and third models, and the concentration increases distally to stenosis where it seems shear stress has decreased, although no vortex has formed. Figure 12 shows maximum shear stress variations for the third model. As can be seen in Fig. 12, the change of shear stress values is much in the stenosis region

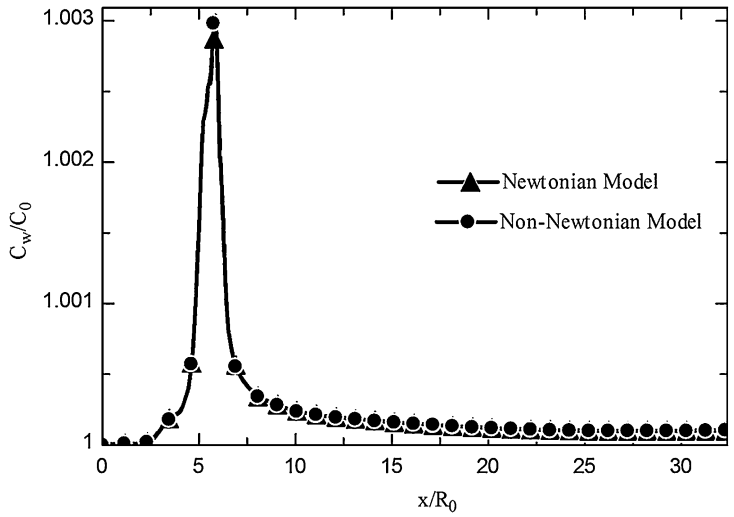

Fig. 11. Axial LSC variations for the fluid-wall Newtonian and non-Newtonian models.

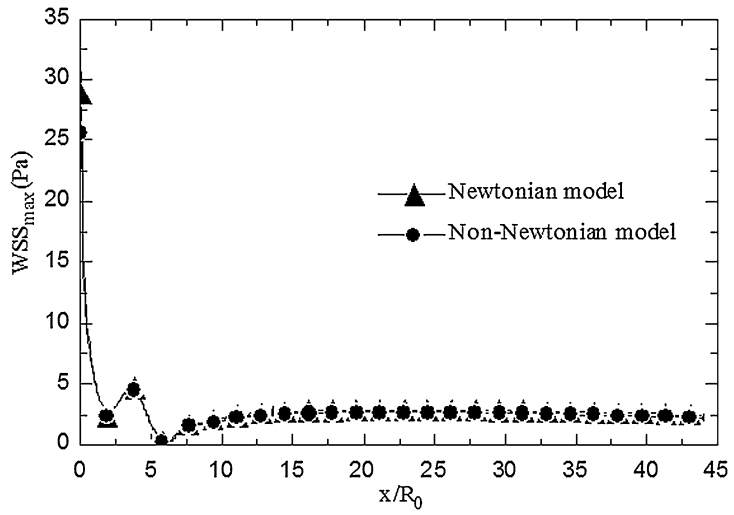

Fig. 12. Time-average maximum WSS along arterial wall for the third model.

while these variations decrease after the stenosis region. By comparison between Figs 11 and 12, it can be seen that LSC increases in the regions that shear stress reaches to minimum value. Time averaged concentration profiles within the wall in the stenosis region are also shown in Fig. 13. In this case, the filtration velocity is an unknown parameter and must be calculated. Figure 14 shows the filtration velocity along the wall. In the vicinity of the stenosis region, a decrease in cross section of the artery resulted in diminution of the pressure and consequently filtration velocity increase. Then by increasing cross section and accordingly pressure, velocity decreases and after the stenosis, it reaches an almost to a constant value. As can be seen in Figs 9 and 10, the values of LSC for wall-free model are more than the values for the fluid-wall model. Comparison between the maximum wall shear stresses of both models shown in Fig. 15 confirms this result because the wall shear stress values for wall-free model are less than the values of the fluid-wall model.

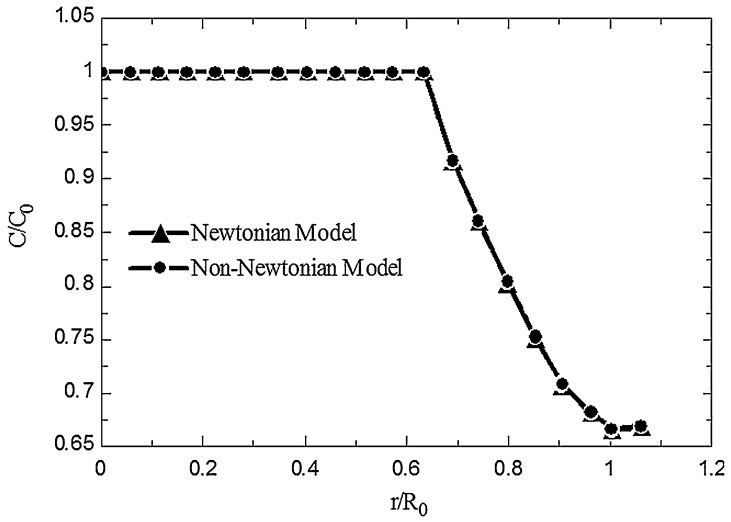

Fig. 13. Time-average concentration variations within wall for the third model.

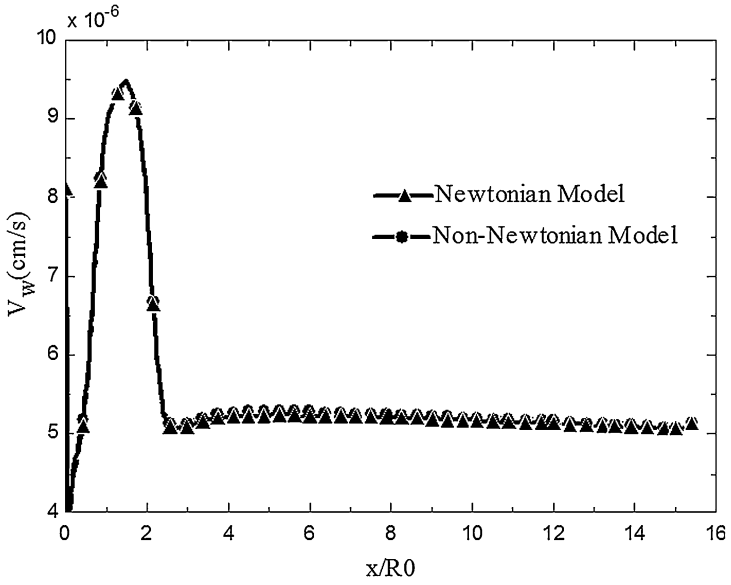

Fig. 14. Time-average filtration velocity along the arterial wall.

As Figs 9–11 confirm the values of LSC for Newtonian fluid are more than non-Newtonian fluid. It seems that shear stress as an effective factor has appeared here and the more shear stress values for the non-Newtonian fluid have caused this result. Although difference of the LDL concentration between Newtonian and non-Newtonian models in the third model is not considerable. It seems that low shear stress difference between Newtonian and non-Newtonian models could be a reason (Fig. 12). The shear stress values of the non-Newtonian fluid for the wall-free model are less than the values for the fluid-wall model. Hence, the values of LSC in the wall-free model are more than another model. Figure 13 shows concentration variations within the wall for Newtonian and non-Newtonian models. Actually, because

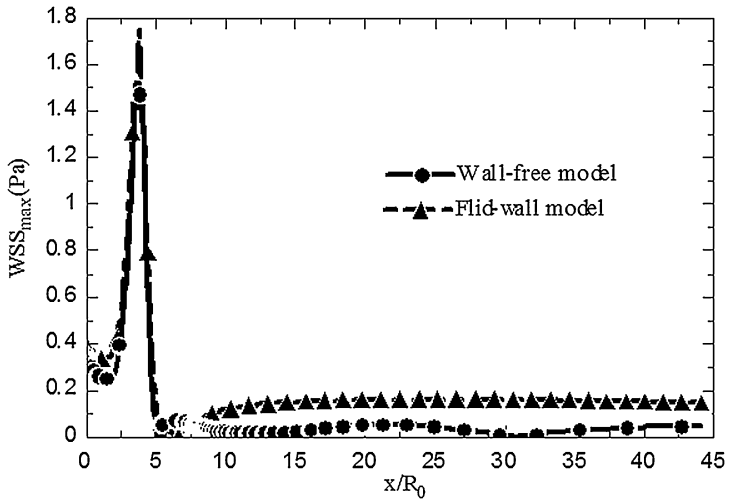

Fig. 15. Maximum wall shear stress for Newtonian fluid in wall-free (first model) and fluid-wall (second model).

of low permeation of fluid into the wall, the effectiveness of Newtonian or non-Newtonian assumption of fluid on LDL concentration is not considerably enough.

5. Conclusions

Three models of arterial stenosis with and without considering effects of FSI to investigate the LDL transport under pulsatile flow are simulated. In this study, LSC variations for the Carreau non-Newtonian fluid model are compared by Newtonian model. The simulation results confirm the significant effect of FSI on the LDL transport. In addition, the effects of the non-Newtonian on LSC assumption of blood fluid are considerable for the first and second models, especially in stenosis region where there are most variations. However, the effect of this assumption on LDL concentration into the wall is not negligible in these models, while in the third model, the effects of non-Newtonian assumption are unimportant.

Conflict of interest

The authors have no conflict of interest to report.

References

[1] study ECftaca, Endarterectomy for asymptomatic carotid artery stenosis, *American Medical Association* **273** (1995), 1421–1428. doi:10.1001/jama.1995.03520420037035.

[2] R.W. Hobson, W.C. Mackey, E. Ascher, M.H. Murad, K.D. Calligaro, A.J. Comerota, V.M. Montori, M.K. Eskandari, D.W. Massop, R.L. Bush, B.K. Lal and B.A. Perler, Management of atherosclerotic carotid artery disease: Clinical practice guidelines of the society for vascular surgery, *Journal of vascular surgery: official publication, the Society for Vascular Surgery [and] International Society for Cardiovascular Surgery, North American Chapter* **48** (2008), 480–486.

[3] M. Prosi, P. Zunino, K. Perktold and A. Quarteroni, Mathematical and numerical models for transfer of low-density lipoproteins through the arterial walls: A new methodology for the model set up with applications to the study of disturbed lumenal flow, *Biomechanics* **38** (2005), 903–917. doi:10.1016/j.jbiomech.2004.04.024.

[4] N. Fatouraee, X. Deng, A. De Champlain and R. Guidoin, Concentration polarization of low-density lipoproteins (LDL) in the artenal system, *Ann. N. Y. Acad. Sci.*, **858** (1998), 137–146.
[5] A. Nematollahi, E. Shirani, I. Mirzaee and M.R. Sadeghi, Numerical simulation of LDL particles mass transport in human carotid artery under steady state conditions, *Scientia Iranica* **19** (2012), 519–524.
[6] L. Ai and K. Vafai, A coupling model for macromolecule transport in a stenosed arterial wall, *Heat and Mass Transfer* **49** (2006), 1568–1591. doi:10.1016/j.ijheatmasstransfer.2005.10.041.
[7] N. Yang and K. Vafai, Modeling of low-density lipoprotein (LDL) transport in the artery – Effects of hypertension, *Heat and Mass Transfer* **49** (2006), 850–867. doi:10.1016/j.ijheatmasstransfer.2005.09.019.
[8] N. Fatouraee, X. Deng, A. De Champlain and R. Guidoin, Numerical simulation of low-density lipoprotein (LDL) transport from flowing blood to the arterial wall in arterial stenoses, *Biomechanical Engineering* (1999).
[9] W. Liao, T.S. Lee and H.T. Low, Numerical studies of physiological pulsatile flow through constricted tube, *International Journal of Numerical Methods for Heat and Fluid Flow* **14** (2004), 689–713. doi:10.1108/09615530410539991.
[10] Y.I. Cho and K.R. Kensey, Effects of the non-Newtonian viscosity of blood on flows in a diseased arterial vessel. Part 1: Steady flows, *Biorheology* **28** (1991), 241–262. doi:10.3233/BIR-1991-283-415.
[11] B.M. Johnston, P.R. Johnston, S. Corney and D. Kilpatrick, Non-Newtonian blood flow in human right coronary arteries: Steady state simulations, *Journal of Biomechanics* **37** (2004), 709–720. doi:10.1016/j.jbiomech.2003.09.016.
[12] S.L. Wilens and R.T. McCluskey, The comparative filtration properties of excised arteries and veins, *The American Journal of the Medical Sciences* **224** (1952), 540–547. doi:10.1097/00000441-195211000-00009.
[13] A. Valencia and M. Villanueva, Unsteady flow and mass transfer in models of stenotic arteries considering fluid-structure interaction, *Heat and Mass Transfer* **33** (2006), 966–975. doi:10.1016/j.icheatmasstransfer.2006.05.006.
[14] S.F. Tsai and T.W.H. Sheu, Finite-element analysis of incompressible Navier–Stokes equations involving exit pressure boundary conditions, *Numerical Heat Transfer, Part B: Fundamentals* **39** (2001), 479–507. doi:10.1080/104077901750188859.
[15] K.M. Khanafer, J.L. Bull and R. Berguer, Fluid-structure interaction of turbulent pulsatile flow within a flexible wall axisymmetric aortic aneurysm model, *European Journal of Mechanics – B/Fluids* **28** (2009), 88–102. doi:10.1016/j.euromechflu.2007.12.003.
[16] K.J. Bathe, *Computational Fluid and Solid Mechanics*, Vol. **1**, Elsevier Science, 2001.
[17] M. Kaviany, Conduction heat transfer, in: *Principles of Heat Transfer in Porous Media*, Mechanical Engineering Series, Springer US, 1991, pp. 115–151. doi:10.1007/978-1-4684-0412-8_3.
[18] D.A. Nield and A. Bejan, *Convection in Porous Media*, Springer, 2006.
[19] H. Teng and T.S. Zhao, An extension of Darcy's law to non-Stokes flow in porous media, *Chemical Engineering Science* **55** (2000), 2727–2735. doi:10.1016/S0009-2509(99)00546-1.
[20] A.M. Britto and M.J. Gunn, *Critical State Soil Mechanics Via Finite Elements*, E. Horwood; Halsted Press, Chichester, West Sussex; New York, 1987.
[21] J.S. Johnson, L. Dresner and K.A. Kraus, Hyperfiltration, in: *Principles of Desalination*, Vol. 1, Academic Press, 1966, pp. 225–230.
[22] S. Fazli, E. Shirani and M.R. Sadeghi, Numerical simulation of LDL mass transfer in a common carotid artery under pulsatile flows, *Biomechanics* **44** (2011), 68–76. doi:10.1016/j.jbiomech.2010.08.025.
[23] P.L. Blackshear, K.W. Bartel and R.J. Forstrom, *Fluid Dynamic Factors Affecting Particle Capture and Retention*, New York Academy of Science, New York, 1977.